Anomalous radial expansion in central heavy-ion reactions

K. Morawetz,[1,2] M. Płoszajczak,[2] and V. D. Toneev[2,3]
[1]*LPC-ISMRA, Boulevard Marechal Juin, F-14050 Caen, France*
[2]*Grand Accélérateur National d'Ions Lourds (GANIL), CEA/DSM – CNRS/IN2P3, BP 5027, F-14076 Caen Cedex 05, France*
[3]*Bogoliubov Laboratory of Theoretical Physics, Joint Institute for Nuclear Research, RU-141980 Dubna, Russia*
(Received 12 July 2000; published 25 October 2000)

The expansion velocity profile in central heavy-ion reactions in the Fermi energy domain is examined. The radial expansion is non-Hubblean and in the surface region it scales proportional to a higher exponent ($\alpha > 1$) of the radius. The anomalous expansion velocity profile is accompanied by a power-law nucleon density profile in the surface region. Both these features of central heavy-ion reactions disappear at higher energies, and the system follows a uniform Hubble expansion ($\alpha \simeq 1$).

PACS number(s): 05.45.−a, 05.20.Dd, 24.10.Cn

I. INTRODUCTION

In heavy-ion (HI) collisions, the stage of compression and heating is followed by the expansion of nuclear matter. Expansion dynamics as a collective motion of excited matter is characterized by certain space-momentum correlations and has been well ascertained by experimental data such as the collective flow. In particular, in central heavy-ion collisions with the beam energy ranging from the Fermi energy to almost 200 GeV/nucleon, the radial flow is clearly manifested through the flattening of the transverse spectra with the particle mass and this effect, as expected, is stronger for heavier systems [1].

The collective expansion scenario is important also in other issues. In studying the quantum statistical correlations which describe the space-time characteristics of expanding systems, one can infer the information about the freeze-out configuration. The recent finding here is that the size parameters of an effective source are determined not only by the geometrical length scale which measures the region of homogeneity [2] but also by the thermal length scale which is related to the region in the coordinate space from which identical particles with similar momenta may emerge [3]. Alongside with the temperature and the freeze-out time, the thermal size of a source is determined by the velocity gradients in this source. The thermal length dominates the correlation function if the geometrical length scale is sufficiently large [3]. Similarly, the question about the particle velocity profile at the freeze-out configuration arises when one considers the formation of light nuclei in the framework of a coalescence model [4].

In almost all papers devoted to this subject, the velocity profile is assumed to be linear:

$$\vec{v} = \frac{\dot{R}(t)}{R(t)} \vec{r}, \tag{1}$$

where $\vec{v}$ and $\vec{r}$ are three- or two-dimensional vectors for the spherically or cylindrically symmetric expansion, respectively. The relation (1) is prompted by an analytical scaling solution of the equations of nonrelativistic hydrodynamics with the ideal gas equation of state for a slowly expanding fireball [5,6]. In fact, Eq. (1) is a consequence of a regular motion governed by the continuity equation when a fluid does not influence the expansion rate. This relation is well known in cosmology where the Hubble constant [7,8] $\dot{R}(t)/R(t) \approx 65$ km/s/Mpc, at the right-hand side of Eq. (1), characterizes the expansion of homogeneous and isotropic galaxies [8].

It is important to note that Eq. (1) need not be valid in general. As was shown by Dumitru [9], while the longitudinal expansion of the fireball three-volume is independent of the energy density of the fluid, the transverse collective motion in the case of (3+1)-dimensional expansion may couple the expansion rate to the properties of the fluid, i.e., to the equation of state. In particular, the hydrodynamic solution for a fireball expanding in the longitudinal and transverse direction with a possible first order hadronization phase transition affects the three-volume expansion rate on the hadronization hypersurface [9].

Analyzing the experimental data on nuclear multifragmentation within an extended statistical microcanonical model which takes into account an interplay of the radial expansion with a nonspherical shape of the fragmenting nucleus [10], it turned out to be necessary to postulate a non-Hubblean velocity profile $\vec{v}(\vec{r})$ for fragments in the freeze-out volume:

$$\vec{v}(\vec{r}) = v_0 \left(\frac{r}{R_0} \right)^{\alpha} \frac{\vec{r}}{r}, \tag{2}$$

with α in between 1.5 and 2 [10], to explain the experimental charge-number dependence of the mean kinetic energy of fragments in central Xe+Sn collisions at 50 MeV/nucleon. The answer to the question of why the exponent α of the radial expansion differs from 1 ($\alpha = 1$ yields the Hubble expansion) cannot be given within the statistical multifragmentation model. An application of the hydrodynamics for this kind of problem is also questionable because the nucleon density at the freeze-out configuration is low and, moreover, the dynamical processes at short time scales are not correctly described. For that reason, in this work we study both the particle velocity profile and the particle density profile in central HI collisions using the framework of a nonlocal

quantum kinetic theory [11]. To gain an insight into the dynamics of the collective expansion of small fermionic systems such as atomic nuclei, the kinetic approach which uses the quasiparticle interaction as input and takes into account consistently the two-particle correlations [11] is probably more reliable, even though the dynamical formation of clusters is absent in this approach.

The paper is organized as follows. In Sec. II A, the main ingredients of the nonlocal quantum kinetic approach are presented. The time evolution of central Ta+Au collisions at 33 and 60 MeV/nucleon is studied in Sec. II B by looking at the transversal and longitudinal profiles of the nucleon velocity, the nucleon density, and the proton to neutron ratio. The expansion velocity profile is discussed in more details in Sec. II C, separately for bulk and surface particles. The qualitative evolution of the radial expansion profile with the collision energy is compared in Sec. II D with the dynamical trajectories of excited system in the temperature-particle density plane. The possible consequences of the long-range tail in the particle density on the small momentum behavior of the Bose-Einstein correlations are discussed in Sec. II E. Finally, Sec. III summarizes the main results of the paper.

II. KINETIC APPROACH

A. Nonlocal quantum kinetic equation

The observables of interest are the particle density $n(r,t)$, the current density $J(r,t)$, and the kinetic energy density $E(r,t)$, which can be expressed by the one-particle phase-space distribution function $f(p,r,t)$ as follows:

$$n(r,t)=\int \frac{dp}{(2\pi)^3} f(p,r,t),$$

$$J(r,t)=\int \frac{dp}{(2\pi)^3} p\ f(p,r,t),$$

$$E(r,t)=\int \frac{dp}{(2\pi)^3} \frac{p^2}{2m} f(p,r,t). \tag{3}$$

The one-particle distribution function obeys a nonlocal Boltzmann-Uehling-Uhlenbeck (BUU) kinetic equation [11]

$$\frac{\partial f_1}{\partial t}+\frac{\partial \varepsilon_1}{\partial k}\frac{\partial f_1}{\partial r}-\frac{\partial \varepsilon_1}{\partial r}\frac{\partial f_1}{\partial k}$$
$$=\sum_b \int \frac{dpdq}{(2\pi)^6} \mathcal{P}[f_3 f_4(1-f_1)(1-f_2)$$
$$-(1-f_3)(1-f_4)f_1 f_2], \tag{4}$$

with Enskog-type shifts of the arguments [11]:

$$f_1 \equiv f(k,r,t),$$

$$f_2 \equiv f(p,r-\Delta_2,t),$$

$$f_3 \equiv f(k-q-\Delta_K,r-\Delta_3,t-\Delta_t),$$

$$f_4 \equiv f(p+q-\Delta_K,r-\Delta_4,t-\Delta_t). \tag{5}$$

The arguments of the effective scattering measure $\mathcal{P}$ are centered in all Δ shifts. The quasiparticle energy ε contains the mean field as well as the correlated self-energy. The shifts or displacements are a compact form of gradient corrections and ensure that the conservation laws contain both the mean-field and the two-particle correlations. In particular, the momentum and the energy gain arises from the finite duration of collisions [12]. All shifts in Eqs. (5) are proportional to derivatives of the scattering phase shift [11,13,14] and have been calculated for realistic nuclear potentials [15]. When neglecting these shifts, one recovers the usual BUU scenario.

It should be noted that using the nonlocal BUU kinetic equations [11] for the description of the proton spectra in central Xe + Sn collisions at 50 MeV/nucleon leads to a significant enhancement of the high energy tail [16] and a better agreement with the experimental data than obtained using the standard BUU equations.

B. Evolution plots

The result of the nonlocal BUU scenario for the reaction Ta+Au at 33 MeV/nucleon can be seen in Figs. 1 and 2. Let us concentrate first on the corresponding velocity and density profiles (the first and second columns in Fig. 1) and the arrows characterizing the mass momentum (the first column in Fig. 2). One sees that at around 40 fm/c the nuclei start to squeeze out the matter side wards (the first column in Fig. 2), which is characterized by the momentum focusing at both sides perpendicular to the beam direction, predominantly in peripheral regions. The surface matter is stopped and bounced back in the longitudinal direction during the times 20–80 fm/c (see the first column in Fig. 1). The inner (bulk) matter exhibiting a quite clear spatial boundary (see the second column in Fig. 2) is still moving inwards. This leads at short time scales ($\sim$40 fm/c) to an enhancement of matter density. The strong velocity gradient, which is seen at 60 fm/c, disappears at about 100 fm/c and the inner matter comes to a rest. The recoil of the splashing matter at the surface and the attractive mean-field force start effectively to reaccelerate the inner matter towards the center of mass. Since the surface particles are still accelerating in the outward direction, there is a zone of matter in between which comes to a rest. This evolution leads to a dumbbell structure in the transversal density profile at 120–240 fm/c.

The different behavior of the surface matter and the bulk matter leads to the development of a nonlinear velocity profile in the surface region, which can be seen in the log-log representation of the angular-averaged velocity in the second column of Fig. 2. For $t>80$ fm/c, the velocity-radius scaling with an asymptotically stable coefficient $\alpha_{surf}\simeq 1.75\pm 0.05$ (see the second column in Fig. 2) appears definitely in the surface region. In this region, the particle density drops nearly as a power law: $n(r)\sim r^{-\beta}$, with the asymptotically stable (for $t>120$ fm/c) coefficient: $\beta\simeq 3\pm 0.2$. As can be seen from the N/Z ratios in the third column in Fig. 1, the Coulomb interaction expels protons from the surface in the early stage of the evolution. In particular, the proton rms radius is larger than the neutron one. This effect becomes weaker at later times ($t\simeq 200$ fm/c) but, nevertheless, it sur-

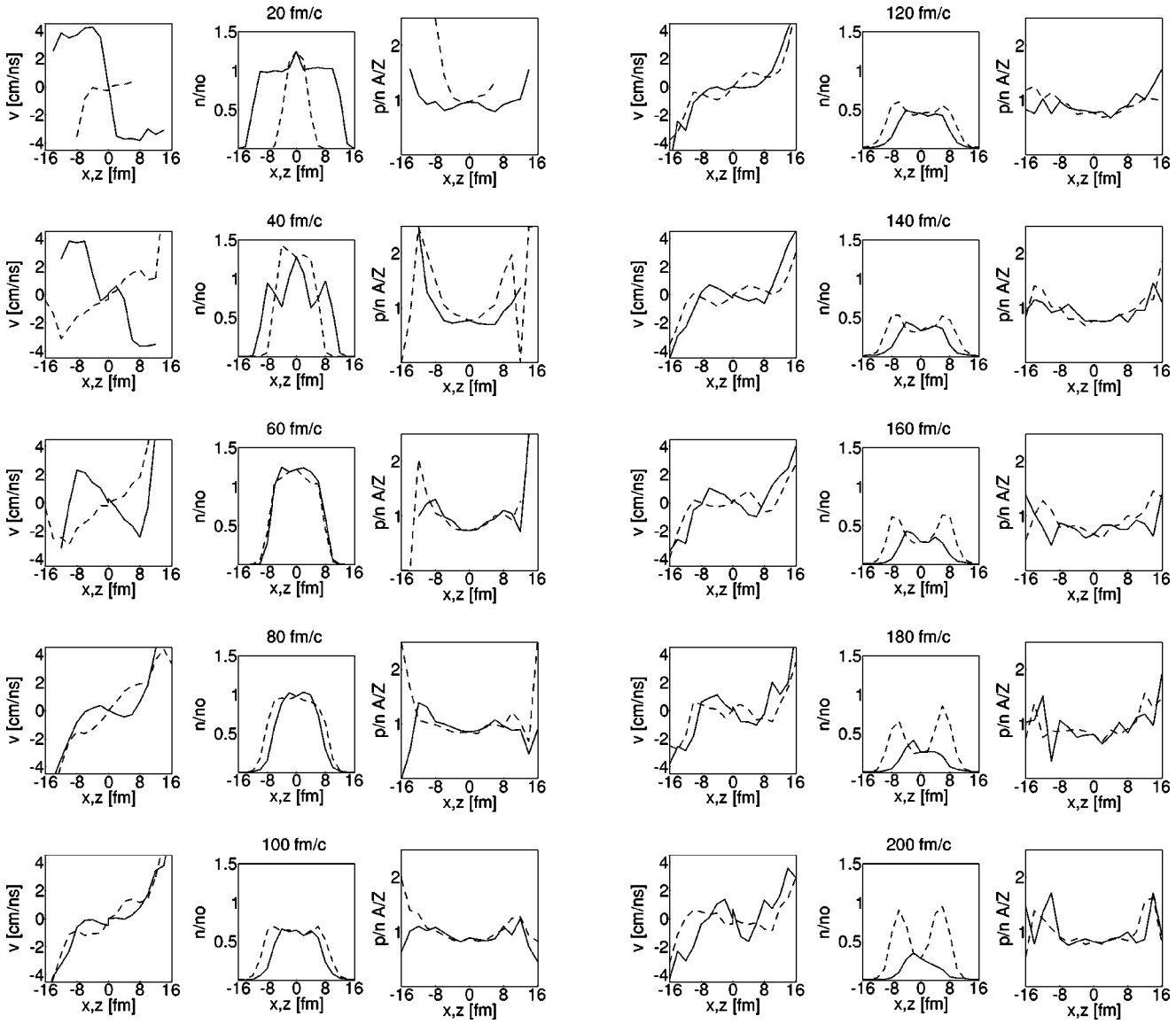

FIG. 1. The time evolution of central Ta+Au collisions at $E_{lab}/A=33$ MeV in the nonlocal kinetic model [12]. The first column represents the velocity profile. Both transversal (the *x* direction) (the dashed line) and the longitudinal (the *z* direction) (the solid line) profiles are shown. The second column shows the longitudinal (the solid line) and the transversal (the dashed line) density profiles in units of fm^{-3}. The third column presents the ratio of proton and neutron densities normalized to the initial Z/A ratio for both the longitudinal (the solid line) and the transversal (the dashed line) projections.

vives, indicating that proton and neutron distributions are different in the surface region. This may lead to different source temperatures and temperature gradients for protons and neutrons and, hence, to different quantum statistical corrections for protons and neutrons in the interferometry experiments. This possibility has been suggested in the phenomenological analysis of the asymmetric reaction Ar+Au at 30 MeV/nucleon [17].

These two unusual effects—the nonlinear velocity profile with $\alpha_{surf}\in[1.5,2.0]$ and an approximately power law fall off of the particle density with $\beta\simeq 3$—characterize the transitional region in the central collisions of symmetric HI collisions in the Fermi energy domain.

For later times ($t>200$ fm/c), one sees the formation of an oblate configuration which is connected to the inversion of the velocity of the inner matter and to the accumulation of the density. In agreement with earlier observations [18,19], we see that the formed hot and nearly fused matter is not spherically symmetric. We would like to remark that this deformation is specific for energies around the Fermi energy and, moreover, is impact-parameter dependent. At nonzero impact parameters, the shape of the matter distribution becomes prolate due to the spectator matter keeping its initial direction of motion and also due to the angular momentum effects.

The evolution picture shown in Figs. 1 and 2 is essentially changed at higher bombarding energies. At $E_{lab}/A=60$ MeV (see Figs. 3 and 4), the time interval where the Coulomb force counterbalances the nuclear forces is becoming very short (e.g., see the plots for $t=40$ fm/c) and the system

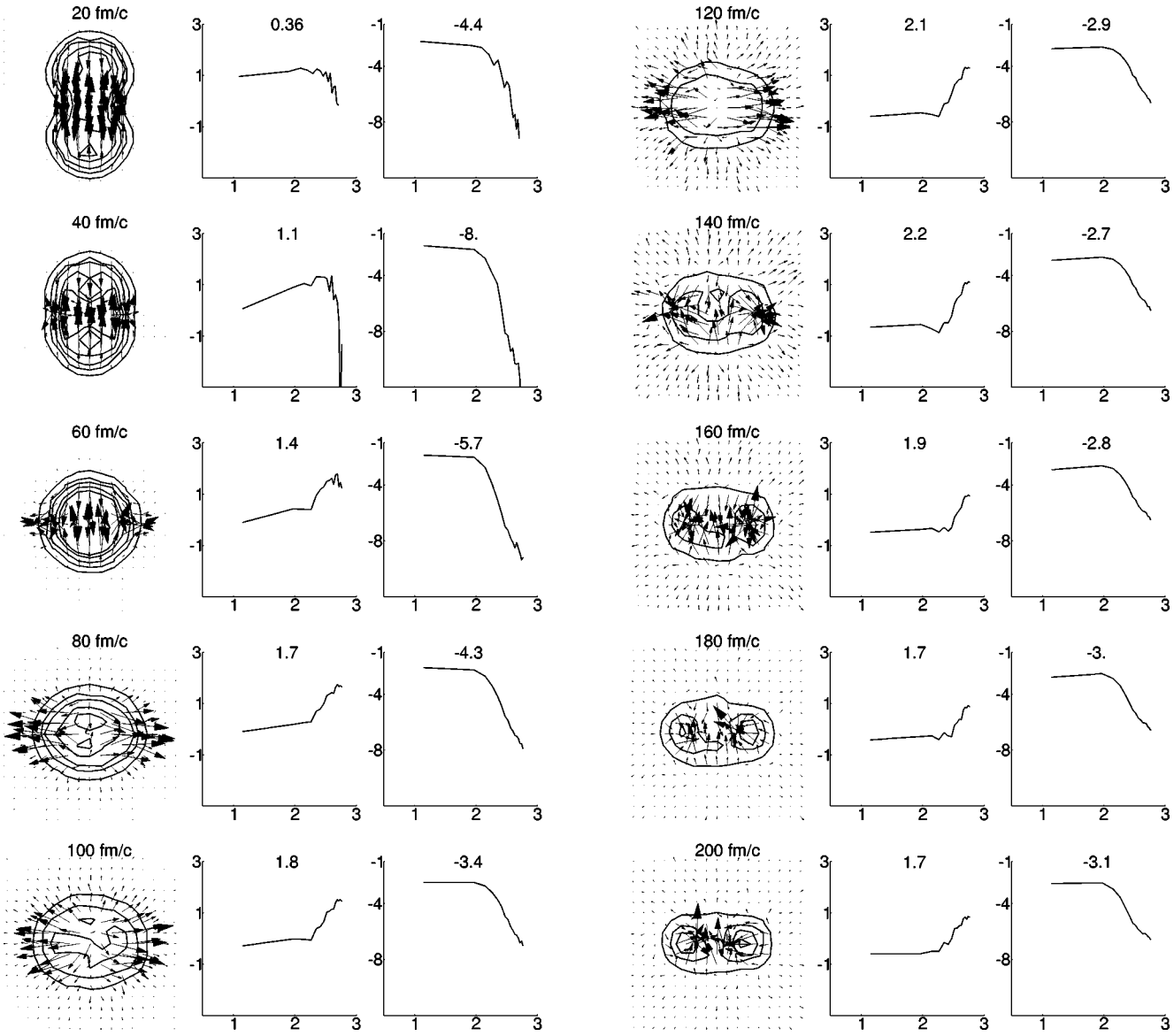

FIG. 2. The time evolution of central Ta+Au collisions at $E_{lab}/A=33$ MeV in the nonlocal kinetic model [12]. Plots in the first column show the $(x-z)$ density cut. The mass momenta are shown by arrows. The second column shows the log-log plot of the angular-averaged modulus of the expansion velocity versus the radius. The slope of the straight line fit of the surface matter expansion profile for $R>10$ fm is indicated at each plot (see also Fig. 5). The third column shows the log-log plot of the angular-averaged nucleon density versus the radius. The slope of the straight line fit of the surface profile is indicated at each plot as well.

enters very fast in the phase of a smooth radial expansion. In this case, the velocity-radius scaling can be well approximated asymptotically by a single exponent $\alpha_{bulk}=\alpha_{surf}\simeq 1$. The particle density is expanding almost uniformly and no characteristic power-law dependence is seen in the surface region. The proton excess in the surface region is less pronounced than at $E_{lab}/A=33$ MeV/nucleon (see Fig. 1) and $Z/N\simeq 1$ at later times. One expects that with increasing bombarding energy in symmetric HI reactions the effective source parameters for protons and neutrons become close to each other.

C. Expansion velocity

Let us now discuss the dependence of the expansion velocity on the radius in more detail. As was noted above, two different slopes can be distinguished at lower collision energies. We call the ''inner'' and ''outer'' parts of the density profile the ''bulk'' and ''surface'' regions, respectively. They are separated here at around $R=10$ fm. Therefore, we plot in Fig. 5 the time dependence of the exponent α in these two regions for different bombarding energies.

Let us start with the reaction at $E_{lab}/A=33$ MeV. The very first stage of the collision, where the nuclei are slightly overlapping, is characterized by similar values of the exponents α in the bulk and the surface regions. This feature continues until the surface particles begin to be evaporated. At around this time, the surface develops a much steeper velocity gradient with α_{surf} as large as ~ 2. At the same time, the bulk matter velocity profile is quite smooth and even α_{bulk} changes the sign [20]. After this overshooting of

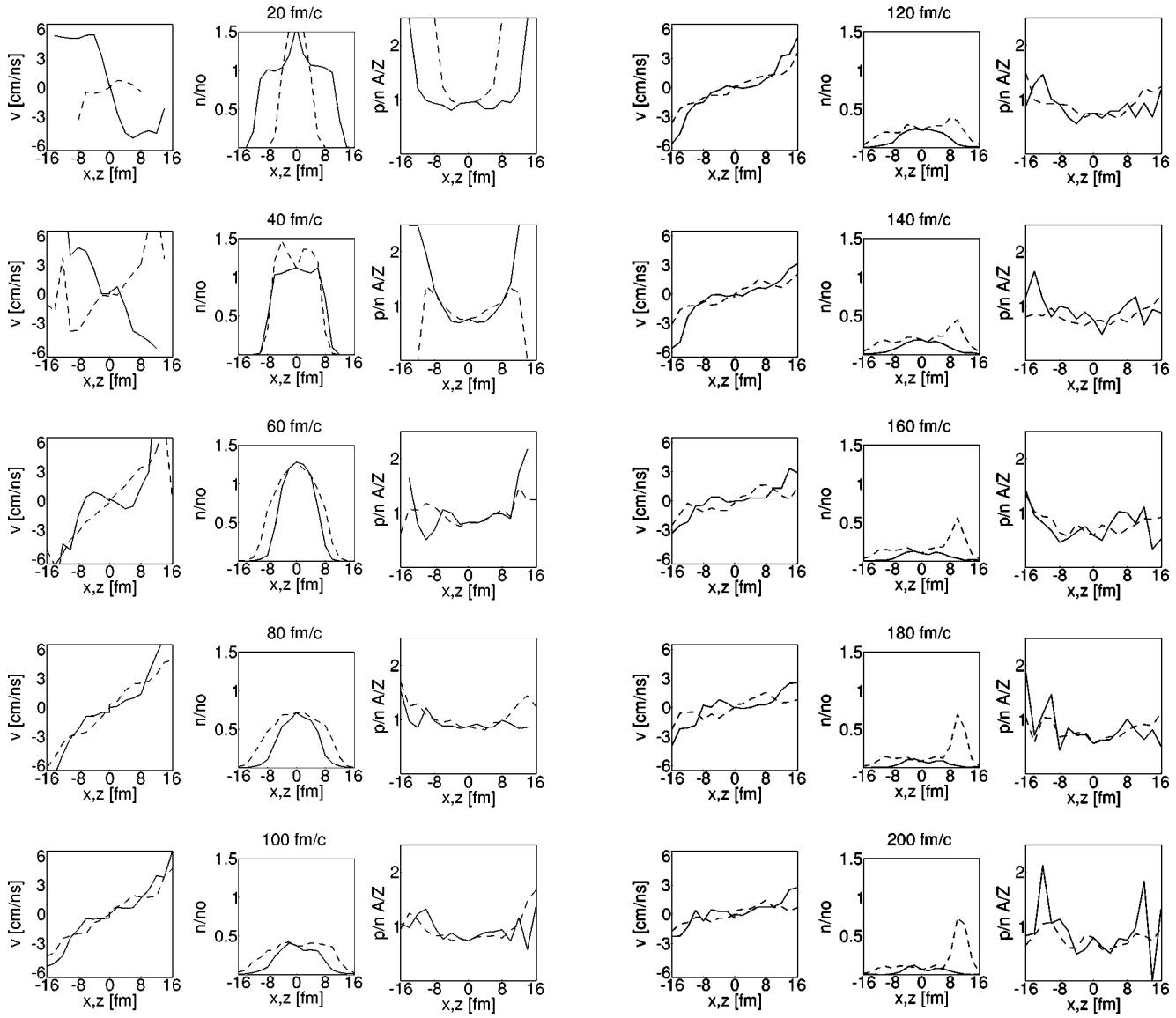

FIG. 3. The same as in Fig. 1 but for $E_{lab}/A=60$ MeV.

the surface exponent during a time interval 100–200 fm/c, the bulk matter develops the radial expansion with the coefficient α_{bulk} which is approaching α_{surf}. Note that even at this stage the mass current is characterized by nonlinear scaling. Hence, using the Hubble ansatz for the radial flow in the analysis of experimental data in the Fermi energy domain is not justified.

At lower energies ($E_{lab}/A=15$ MeV in Fig. 5), one observes that the difference between radial flow patterns in the surface and bulk regions becomes even stronger than at $E_{lab}/A=33$ MeV. Consequently, higher values of the exponent α_{surf} are reached asymptotically. Moreover, we see that a giant resonance with a period of $T=60$ fm/c, or an energy of $2\pi/T=20.6$ MeV is excited. This can be considered as a complete fusion event.

If one proceeds to energies higher than the Fermi energy, one sees that the general trend of evolution is conserved but the deviation between surface and bulk matter expansion patterns decreases; i.e., the coefficients α_{bulk} and α_{surf} become close to one another. One can see also that the maximum value of the exponents α is reached faster than at lower energies, and the exponents α are becoming close to 1 at late times. The nuclear system at this high excitation energy is expanding continuously. As a result of the higher initial velocity, there is practically no inversion of the velocity profile and no time-periodic structures like giant resonances are excited. The Hubble expansion pattern is reached faster and no anomalous behavior ($\alpha_{surf}>1$) is observed for energies higher than 90 MeV/nucleon.

D. Dynamical trajectories

To elucidate the connection of the anomalous velocity profile with the multifragmentation, let us characterize an instantaneous state of the system in terms of the average nucleon density n and the temperature T. In order to define a global time-dependent temperature $T(t)$ we adopt the Fermi liquid relation [21]

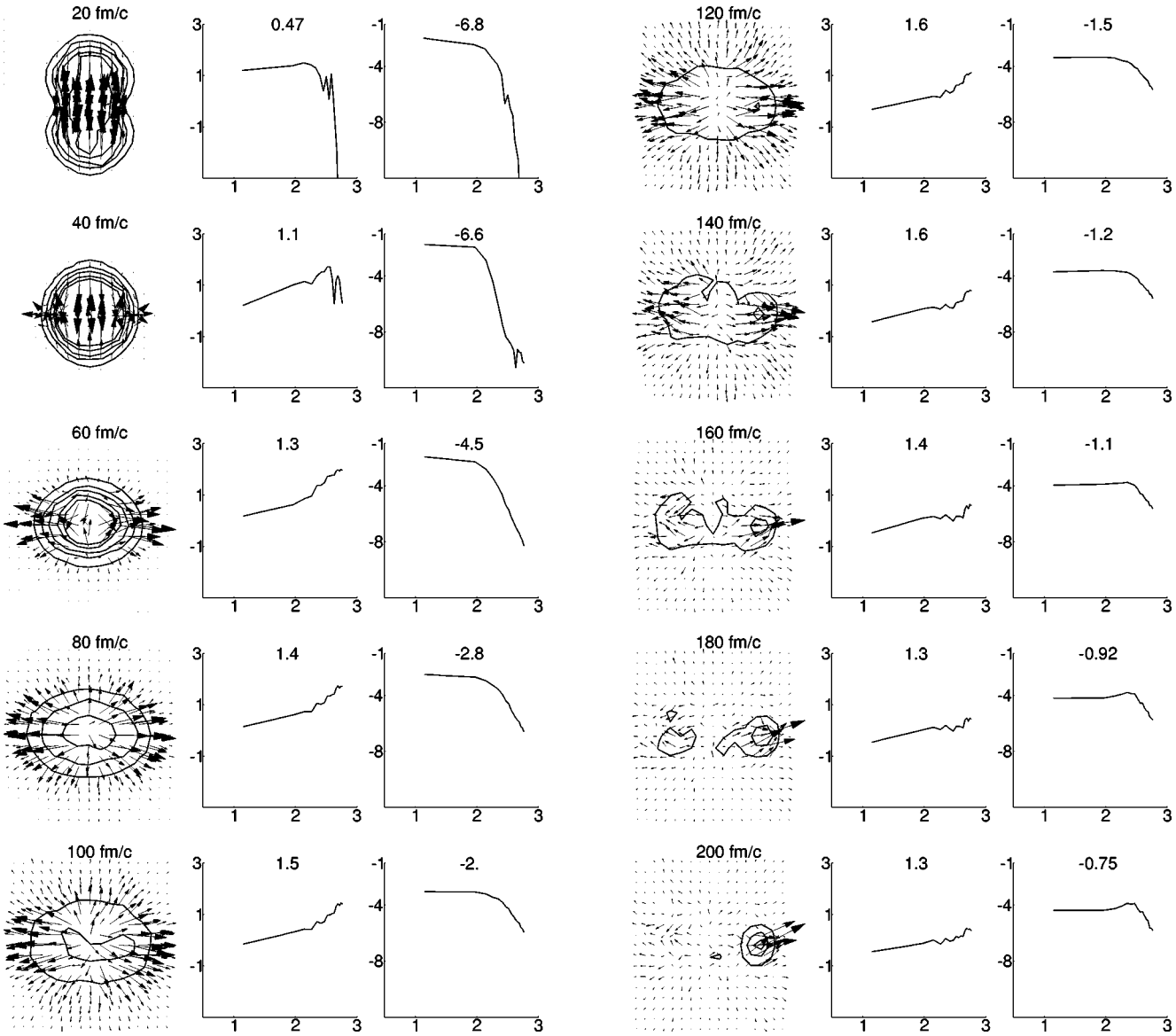

FIG. 4. The same as in Fig. 3 but for $E_{lab}/A=60$ MeV.

$$E(t)=\frac{3}{5}E_F(t)+E_{\rm coll}(t)+\frac{\pi^2}{4E_F(t)}\,T(t)^2, \tag{6}$$

where the global kinetic energy $E(t)$, the collective energy $E_{\rm coll}$, and the Fermi energy $E_F(n)=(3\pi^2 n/2)^{2/3}/2m$ are given by a spatial integration of the local quantities (3):

$$E(t)=\frac{\int dr\, E(r,t)}{\int dr\, n(r,t)},$$

$$E_F(t)=\frac{\int dr\, E_F(n(r,t))\, n(r,t)}{\int dr\, n(r,t)}, \tag{7}$$

$$E_{\rm coll}(t)=\frac{\int dr\, \dfrac{J(r,t)^2}{m\, n(r,t)}}{\int dr\, n(r,t)}.$$

It is more problematical to define a density. We will present here the two possibilities. The first one is to consider the density of matter inside the evolving mean-squared radius. The other possibility is to consider the density of matter contained in the static separation of bulk matter by the radius R found earlier in the velocity profile.

The dynamical trajectories in the $(T-n)$ plane for different collision energies are shown in Fig. 6 for bulk matter ($R<10$ fm). Let us first look at the static density definition inside the bulk region. For $E_{lab}/A=15$ and 33 MeV, the system evolves inside the spinodal region and, therefore, is mechanically unstable. In the time interval between 150 and

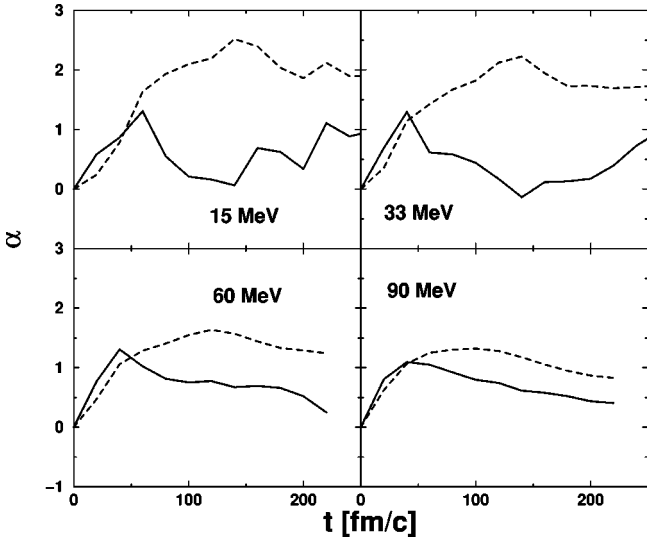

FIG. 5. The exponent α of the power law velocity profile (2) with respect to the radius $v \propto r^{\alpha}$ for different laboratory energies. The dotted lines show the surface matter behavior and the solid lines depict the bulk matter behavior.

200 fm/c, the system is in a configuration with $n \approx n_0/3$ and $T \approx 7-8$ MeV, which are the typical values for the nuclear multifragmentation. At higher energies, the freeze-out density of an evolving system is shifted towards lower densities and finally it ends in a gaseous phase. If one chooses to look at the interior part of the system within the radial size of the mean-squared radius (dotted lines in Fig. 6), the main difference is seen in the initial stage of the evolution where larger nucleon densities are reached but, at the same time, they are passed through much faster. The freeze-out configurations are practically the same as when the above static definition of bulk matter is considered.

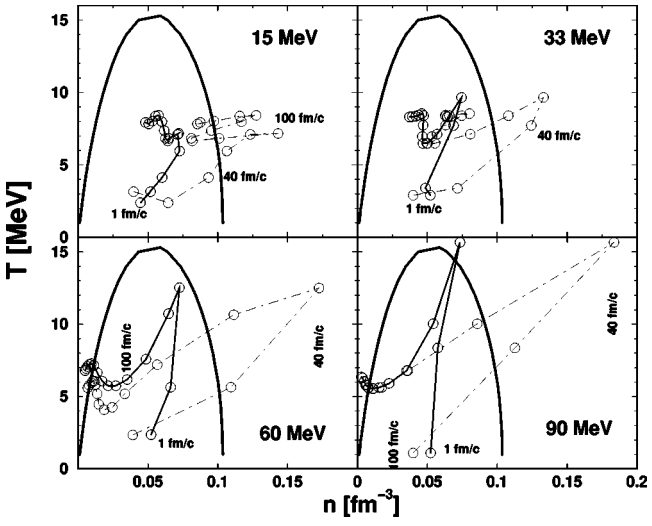

FIG. 6. The time evolution of the temperature versus the density for the sphere of a constant radius ($R<10$ fm) (the solid line), corresponding to the distinction between the bulk and surface regions in Fig. 1, and for the sphere given by the mean-squared radius of the evolving system (the dotted line). The thick solid lines give the limit of the spinodal region for an infinite nuclear matter.

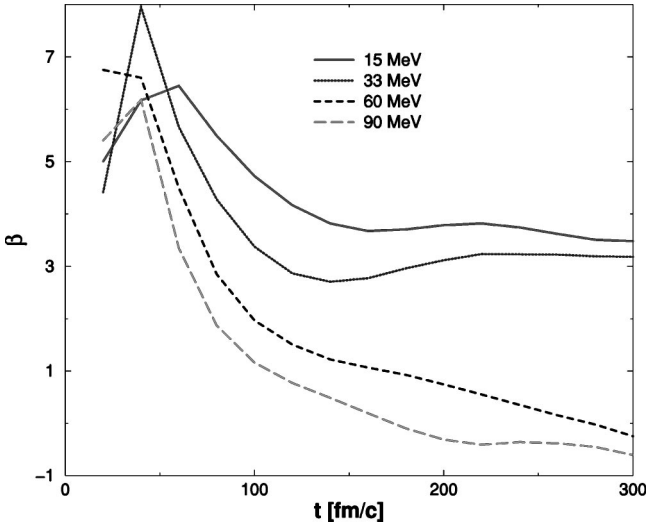

FIG. 7. The time dependence of the exponent β of the power-law fit of the particle density $n \propto r^{-\beta}$ in the surface region ($R>10$ fm) for different collision energies.

E. Long tail of the density distribution

Let us now discuss the particle density profile in more detail. As noted in Fig. 2, the decrease of the particle density in the surface region is algebraic (power law) rather than exponential. In Fig. 7, we plot the time dependence of the exponent β which is extracted from the power law fit: $n(r) \sim r^{-\beta}$, for $R>10$ fm.

There are here two distinct behaviors. For $E_{lab}/A=15$ and 33 MeV, after an initial buildup of the surface region as characterized by the decrease of β in time, the value of exponent β stabilizes asymptotically. The limiting value of β, called β_{lim}, decreases with bombarding energy from $\beta_{lim} \sim 3.5$ at $E_{lab}/A=15$ MeV to $\beta_{lim} \sim 3.1$ at $E_{lab}/A=33$ MeV. Actually, the most interesting long-range region of the nucleon density ends at about $E_{lab}/A \sim 50$ MeV and the smallest value reached is about $\beta_{lim}=2$. In the energy interval 15 MeV $\lesssim E_{lab}/A \lesssim 50$ MeV, the anomalous power-law tail of the nucleon density accompanies the anomalous profile of the expansion velocity in the surface region, and both effects are leading to the non-Gaussian shape of the emitting source and the anomalous short-range correlations.

For energies $E_{lab}/A \geqslant 60$ MeV in the Hubble expansion regime, the exponent β decreases monotonously in time and no asymptotically stable surface region with the power law dependence is seen. At later times, one sees, however, the appearance of a new expansion regime corresponding to the negative values of the exponent β. This indicates the formation of a shell-like structure in the system. The formation time of the shell-like structure decreases rapidly with increasing bombarding energy ($t_{sh} \simeq 280$ fm/c at $E_{lab}/A=60$ MeV and $t_{sh} \simeq 170$ fm/c at $E_{lab}/A=90$ MeV). The β values found are not strongly negative, indicating that the expanding shell is a very diffused object due to the long mean free path of nucleons in the kinetic approach. A similar unusual solution of spherically expanding scaling hydrodynamics has been used in the analysis of the Bose-Einstein correlations [22].

The specific shape fluctuations in the long-range region can be a source of the power-law Bose-Einstein correlations. This problem has been discussed by Białas [23,24] in the context of strong interaction physics at relativistic energies. The long tail of the particle density for the systems produced in the symmetric heavy-ion collisions in the Fermi energy domain may result in unusual quantum statistical correlations. The N-particle interferometry reduced densities can be written as

$$D_N(k_1,\ldots,k_N)=\int dx_1\cdots\int dx_N\Bigg(\sum_{per}\exp[i(x_1p_{a_1}+\cdots+x_Np_{a_N})]\Bigg)n_N(x_1,\ldots,x_N)\times\Bigg[N!\Bigg(\int dx n_1(x)\Bigg)^N\Bigg]^{-1}, \tag{8}$$

where n_N is the N-point density of emitting sources and the sum runs over all permutations of the indices a_i. The above formula supposes the incoherent emission from the source and neglects the final state interaction. In the case of uncorrelated emission in space-time,

$$n_N(x_1,\ldots,x_N)=n_1(x_1)\cdots n_1(x_N),$$

the N-particle cumulant can be written using the Fourier transform of the source density $n_1(x)$ [23]:

$$n_N(k_1,\ldots,k_N)=\sum n_1(k_1-k_{a_1})\cdots n_1(k_N-k_{a_N}), \tag{9}$$

where the sum runs over all permutations of the indices a_i with $a_i\neq i$. If the source density has a power-law tail,

$$n_1(x)\simeq x^{-\beta}\equiv x^{\gamma-D}, \tag{10}$$

its Fourier transform shows also a power law in some range of small momenta [23]:

$$n_1(k)\simeq|q|^{-\gamma}. \tag{11}$$

Thus there is the relation between the power-law tail in the source density distribution and the power law in the two-particle Bose-Einstein correlations which are given in terms of the Fourier transform of the source density:

$$C_2(q)\simeq|q|^{-2\gamma}. \tag{12}$$

Similarly, the higher order cumulants $C_i(q)$ $(i=3,\ldots)$ are expected also to have a power-law dependence on the rescaling of momenta with an index $i\gamma$.

A particularly interesting case of the Bose-Einstein correlations, increasing as the power of $|q|$, corresponds to $\gamma>0$ $(\beta<D)$ in Eq. (10). In the case of central heavy-ion collisions, our analysis suggests that this effect could be seen in symmetric systems for energies 35 MeV$\lesssim E_{lab}/A\lesssim$50 MeV.

III. SUMMARY AND OUTLOOK

The dynamical behavior of heavy-ion reactions in the Fermi energy domain during the first 200 fm/c is clearly associated with a nonlinear $(\alpha>1)$ radial velocity profile (2). The existence of such a non-Hubble radial expansion at the freeze-out configuration was postulated by Le Févre *et al.* [10] in the analysis of experimental kinetic energies of fragments in the Xe+Sn reaction at $E_{lab}/A=50$ MeV in the framework of the statistical microcanonical model. The present studies using the nonlocal kinetic theory show that indeed such an unusual radial flow velocity profile is a plausible freeze-out configuration for symmetric heavy-ion collisions. One can roughly determine the instant of time when the compression turns into the expansion by looking at the crossing point of the bulk α_{bulk} and surface α_{surf} scaling exponents. While at the compression stage these two exponents are almost equal, the expansion stage exhibits a larger exponent for the surface matter than for bulk matter and α_{surf} takes values significantly larger than 1. This dynamical behavior of the surface matter disappears for energies significantly higher than the Fermi energy.

For central heavy-ion collisions in the Fermi energy domain, we see that the expansion stage is characterized by very small values of the exponent α in the bulk ($\alpha_{bulk}\in[0,1]$), indicating its slow evolution and possible mechanical instabilities. At these energies, the system spends a long time in the spinodal region, which may result in its multifragmentation decay. With increasing collision energy, the system passes quickly through this unstable region or, at even higher energies, its thermodynamic trajectories go above the spinodal region. In this case, the multifragmentation due to the spinodal instabilities is hardly possible [25]. For details see [21].

The nonlinear radial velocity profile in the surface region is accompanied by the long tail of the particle density. Both these effects may have important consequences on the quantum statistical correlations and their evolution with the bombarding energy. The effects of the radial expansion on the two-particle correlations have been studied assuming the linear scaling solution $(\alpha=1)$ of the scaling hydrodynamics [3,17]. It was found that the expansion makes the effective radius of the two-particle correlation functions smaller than the geometrical size of the source. We expect this effect to be even stronger in the presence of nonlinear radial expansion flow, leading to an even stronger discrepancy between the effective radius and the geometrical radius. Moreover, the commonly used Gaussian approximation for the source shape is certainly hazardous in this non-Hubble expansion regime. The existence of the power law tail in the particle density can in turn lead to the power-law two-particle Bose-Einstein correlations at small relative momenta of the particles in the range of collisions energies 35 MeV$\lesssim E_{lab}/A\lesssim$50 MeV. It should be stressed that the ratio Z/N in the surface region is strongly different from 1, in particular at early collision times and at low bombarding energies

($E_{lab}/A \lesssim 60$ MeV). This specific effect in the Fermi energy domain, which leads to an effective increase of the proton rms radius and to the change in the temperature gradients in proton/neutron source, may have measurable consequences in the quantum statistical correlations for protons and neutrons. This effect has been studied by Helgesson *et al.* [17] assuming a linear scaling solution ($\alpha=1$) of hydrodynamics for asymmetric HI reactions at 30 MeV/nucleon. Our results suggest that the simultaneous description of n and p spectra, as well as nn and pp correlation functions, may require different source parametrizations for neutrons and protons, though the detailed dynamics for HI reactions at $E_{lab}/A \simeq 30$ MeV is very different from that assumed by Helgesson *et al.* [17]. It is interesting to notice that the nonlocal kinetic theory predicts the appearance of the solution somewhat similar to the linear scaling solution ($\alpha=1$) of hydrodynamics with $\beta<0$ [22] for higher energies bombarding energies ($E_{lab}/A \gtrsim 60$ MeV).

The different behavior of the surface and bulk matter before equilibration can also be of importance for the description of supernovas where a surfacelike ring of matter (crust) is expanding with enormous velocities and is clearly separated from the remaining bulk matter collapsing back into neutron stars. The clearest experimental observation of the expanding shell-like structure noted above comes from stellar astronomy. The envelope material ejected by the stars forms an expanding shell of gas that is known as a planetary nebula. The space-time evolution of these objects is in many aspects similar to the considered evolutions: $\alpha \lesssim 2$, $\beta>0$ and $\alpha \sim 1$, $\beta<0$. The latter solution can be successfully simulated by a scaling solution of the nonrelativistic hydrodynamics [22].

We suggest that the anomalies found in the kinetic expansion reflect the nature of effective interactions among the elementary constituents of the system. Their manifestation is twofold. First, the interplay between the repulsive Coulomb interaction and the attractive mean field results in the formation of a rather sharp surface of the system. Second, the evolution of the bulk matter is not a simple uniform expansion of a homogeneous ideal fluid. In the unstable spinodal region, the local interaction of quasiparticles in the bulk phase affects noticeably the subsequent evolution of the system. In this respect, one should stress again an attractive possibility of implementing both the nonlinear velocity profile and the algebraic long-range density tail into the analysis of the Bose-Einstein correlations. These effects are not only important for the nuclear multifragmentation process but also for the hadron interferometry at ultrarelativistic collisions where the deconfinement phase transition can have a strong influence on the expansion stage. This is of particular interest for the statistical mixed phase equation of state which gives the crossover type of the deconfinement phase transition and allows for a small admixture of unbound quarks at the freeze-out point [26].

An interesting example which illustrates an important difference between the linear and quadratic scalings of the expansion velocity with the radius can be found in cosmology [7]. If there is an attractive force decreasing as an inverse power of the radius, the equation of motion for a radially symmetric matter follows from the total energy h which reads

$$\frac{m}{2}\dot{R}(t)^2 - \frac{G}{R(t)^{\delta}} = h. \tag{13}$$

Assuming a homogeneous matter density n, the mass is $m = 4\pi n R^3/3$. In the case of the escaping matter ($h=0$), one gets

$$\dot{R}(t) = \sqrt{\frac{6G}{4\pi n}} R(t)^{(3-\delta)/2}, \tag{14}$$

what corresponds to taking

$$\alpha = \frac{3-\delta}{2} \tag{15}$$

in Eq. (2). We see that $\delta=1$ for the Coulomb or gravitational forces and, hence, the Hubble expansion ($\alpha=1$) follows in these cases. However, if $\alpha=2$, as found in the surface region of nuclei formed in central HI collisions at around the Fermi energy (see Fig. 5), the above relations lead to a stringlike force with $\delta=-1$. Since this force is used to describe the confinement in the effective theories motivated by the quantum chromodynamics, its occurrence as a consequence of the *dynamical behavior* is worthy of attention. As was shown above in the solution of nonlocal kinetic equations, the interplay between Coulomb and mean field leads to such a stringlike behavior for surface particles. This is here a clear nonequilibrium effect. The above discussed oscillation in the time dependence of the α exponent may be considered as a possible manifestation of this effective dynamical stringlike force in the surface region.

Perhaps the best way to demonstrate the existence of both the non-Hubble radial expansion and the algebraic long-range tail of the particle density would correspond to finding a non-Gaussian deformation of the source in the Bose-Einstein interference experiments for central, symmetric heavy-ion reactions in the narrow range of collision energies ($35\ \text{MeV} \lesssim E_{lab}/A \lesssim 50$ MeV). In the same narrow range the unusual scale dependence of the many-particle correlations at small momenta should be induced via the same Bose-Einstein quantum interference effect if the source has an algebraic (power law) density tail (Sec. II E). On the other hand, as discussed in [10], the kinematical observables related mainly to the intermediate mass fragments provide an independent and sensitive measure of the velocity profile in the deformed, expanding source. To put together all these different pieces of evidence into circumstantial proof for the non-Hubble collective expansion of nuclear aggregates remains a difficult and exciting challenge for future experimental and theoretical studies of heavy-ion collision in the Fermi energy domain.

ACKNOWLEDGMENTS

This work was supported by the IN2P3-JINR agreement No 0049. K.M. would like to thank the LPC for hospitality and a friendly atmosphere.

[1] P. Danielewicz, Nucl. Phys. **A661**, 82c (1999).
[2] A.N. Makhlin and Y.M. Sinyukov, Z. Phys. C **39**, 69 (1988).
[3] T. Csörgo, B. Lörstad, and J. Zimányi, Phys. Lett. B **338**, 134 (1994); T. Csörgo and B. Lörstad, Phys. Rev. C **54**, 1390 (1996); B. Tomásik and U. Heinz, Eur. Phys. J. C **4**, 327 (1998).
[4] A. Polleri, I.N Mishustin, and J.P. Bondorf, Phys. Lett. B **419**, 19 (1998).
[5] J.P. Bondorf, S.I.A. Garpman, and J. Zimány, Nucl. Phys. **A296**, 320 (1978).
[6] P. Csizmadia, T. Csörgo, and B. Lukás, Phys. Lett. B **443**, 21 (1998).
[7] M. Harwit, *Astrophysical Concepts* (Wiley, New York, 1973).
[8] Ch.W. Misner, K.S. Thorne, and J.A. Wheeler, *Gravitation* (Freeman, San Francisco, 1972).
[9] A. Dumitru, Phys. Lett. B **463**, 138 (1999).
[10] A. Le Févre, M. Płoszajczak, and V.D. Toneev, Phys. Rev. C **60**, 051602(R) (1999).
[11] V. Špička, P. Lipavský, and K. Morawetz, Phys. Lett. A **240**, 160 (1998).
[12] P. Lipavský, V. Špička, and K. Morawetz, Phys. Rev. E **59**, R1291 (1999).
[13] P. J. Nacher, G. Tastevin, and F. Laloe, Ann. Phys. (Leipzig) **48**, 149 (1991).
[14] M. de Haan, Physica A **164**, 373 (1990).
[15] K. Morawetz, P. Lipavský, V. Špička, and N. Kwong, Phys. Rev. C **59**, 3052 (1999).
[16] K. Morawetz *et al.*, Phys. Rev. Lett. **82**, 3767 (1999).
[17] J. Helgesson *et al.*, Phys. Rev. C **56**, 2626 (1997).
[18] B. Borderie, B. Remaud, M. Rivet, and F. Sebille, Phys. Lett. B **302**, 15 (1993).
[19] P. Danielewicz, Phys. Rev. C **51**, 716 (1995).
[20] We have checked that such a bouncing back effect is more pronounced in the standard BUU calculations than in the nonlocal kinetic scenario.
[21] K. Morawetz, Phys. Rev. C **62**, 044606 (2000).
[22] T. Csörgo, nucl-th/980911; hep-ph/0001233.
[23] A. Białas, Acta Phys. Pol. B **23**, 561 (1992); A. Białas and B. Ziaja, *ibid.* **24**, 1509 (1993).
[24] P. Bożek, M. Płoszajczak, and R. Botet, Phys. Rep. **252**, 101 (1995).
[25] This does not exclude certainly that the system can be in the spinodal instable region for larger impact parameters.
[26] E.G. Nikonov, A.A. Shanenko, and V.D. Toneev, Heavy Ion Phys. **8**, 89 (1998); V.D. Toneev, E.G. Nikonov, and A.A. Shanenko, in *Nuclear Matter in Different Phases and Transitions*, edited by J.-P. Blaizot, X. Campi, and M. Płoszajczak (Kluwer Academic, Dordrecht, 1999), p. 309.